Pergamon

Neuroscience Vol. 59, No. 1, pp. 21–31, 1994
Elsevier Science Ltd

0306-4522/94 $6.00 + 0.00

MULTIPLE DYNAMICAL MODES OF THALAMIC RELAY NEURONS: RHYTHMIC BURSTING AND INTERMITTENT PHASE-LOCKING

X.-J. WANG*

Department of Mathematics and The James Franck Institute, University of Chicago, 5734 S. University Ave., Chicago, IL 60637, U.S.A.

Abstract—A model of thalamocortical relay neuron is studied to assess whether a 7–14 Hz (spindle) oscillation and a 0.5–4 Hz (delta) oscillation may result from the interplay between a T-type calcium current and a non-specific cation sag current. With moderate change of membrane parameter values, the model neuron can exhibit both the spindle and delta rhythms, at different levels of hyperpolarization; only the slower (delta) one or none. In the case when the model neuron is not intrinsically oscillatory, its response to rhythmic hyperpolarization is complex, and displays the "intermittent phase-locking" phenomenon where bursts of Na^+ action potentials occur infrequently but their occurrence is phase-locked to the rhythmic input.

The rhythmic bursting, whenever possible, is shown to emerge (bifurcate) from a subthreshold oscillation. Near the bifurcation chaotic discharge patterns are observed, where spikes occur intermittently at randomly chosen cycles of a mostly subthreshold slow oscillation. Furthermore, when both the spindle and delta modes can be realized, the transition between the two appears as a sudden drop of the rhythmic frequency with increased hyperpolarization.

The T-type calcium current and the sag current may explain the "intermittent phase-locking" phenomenon that is characteristic to thalamic relay neurons during spindle oscillation and provide a cellular basis for the 7–14 Hz rhythm and the slower 0.5–4 Hz rhythm.

A multitude of ionic conductances endow neurons with the ability to display more than one form of spontaneous activity, as well as input–output relations.[15] An example is the cortically projecting relay neurons in the mammalian thalamus. Thalamic relay neurons respond to sensory inputs by tonical firing of action potentials, in awake and behaving conditions. On the other hand, these cells are known to provide rhythmic drives for certain brain waves in the cortex. They display "10 Hz" (7–14 Hz) spindle oscillations in the early stages and "3 Hz" (0.5–4 Hz) delta oscillations in the deep stages of quiet sleep. Together with the resting state and tonic firing, thalamic relay cells can display at least four types of dynamic modes.

Experiments in recent years have revealed cellular mechanisms responsible for this variety of dynamic modes in thalamic relay cells,[30] as well as neuromodulatory mechanisms for transitions from one state to another.[17] A T-type calcium current (I_T) has been identified to be a key cellular property to the 10 Hz rhythmogenesis, since it imparts the possibility of neuronal bursting discharges at this frequency range.[6,11,12] I_T is de-inactivated by hyperpolarization, thus providing an ionic basis for the so-called post-inhibitory rebound excitation. In principle, a thalamic relay cell endowed with a sufficiently strong I_T can display 10 Hz oscillations under constant injected current (termed intrinsic oscillation). Partial evidence for this has been found in a brain slice preparation of the lateral habenular nucleus of guinea-pig.[37] It is possible, however, that most relay cells in most nuclei of the thalamus do not oscillate intrinsically at 10 Hz. Indeed, during *in vivo* 10 Hz spindling, thalamic relay cells in many major nuclei receive rhythmic inhibitory postsynaptic potentials from the thalamic reticular nucleus, which may be necessary in inducing 10 Hz oscillations in those cells. (Incidently, the habenula is one of the few nuclei which are not connected with the reticular nucleus, and which in fact do not display oscillations of the spindle form.)

More recent *in vitro* preparations uncovered that thalamic relay cells can also display an intrinsic oscillation at 0.5–4 Hz, similar to the delta sleep rhythm.[14,20,25] This "3 Hz" bursting is primarily due to the interplay between a T-type calcium current I_T, and a non-specific cation "sag" current (I_h) which has much slower kinetics than I_T and is activated by hyperpolarization. *In vivo* studies confirmed this finding,[5] and found that gradual hyperpolarization of those cells could induce a transition from the 10 Hz spindle to the 3 Hz delta oscillation.[22,28] Therefore, our present knowledge suggests that although all thalamic relay cells can probably display a tonic firing mode (upon depolarization) and a bursting mode (upon hyperpolarization), they may yet be divided into three types according to their ability of intrinsic oscillations: (I) those which do not oscillate; (II) those

*Present address: Department of Mathematics, University of Pittsburgh, Pittsburgh, PA 15260, U.S.A.

Abbreviations: LTS, low threshold spike.

which can oscillate only at 3 Hz; and (III) those which can oscillate both at 10 and 3 Hz.

This study presents a simple model of the thalamic relay neuron and looks at what conditions produce the three types of behaviors, and also describes their dynamic properties.

COMPUTATIONAL PROCEDURES

The T-type calcium current (I_T) and the sag current (I_h) are largely responsible for the subthreshold properties and slow oscillations of thalamic relay cells. Voltage-clamp data are available for these two currents, which support the present modeling work. In addition, the model contains a sodium current (I_{Na}) and a potassium current (I_K) of the Hodgkin–Huxley type, as well as a persistent (non-inactivating) sodium current ($I_{Na(P)}$) for the spike generation, and a leakage current (I_L). We shall not include other potassium currents known to exist in thalamic relay cells, as they may be important only for fine tuning the membrane dynamics (see Discussion). We use a one-compartment model, which does not consider the morphology of these cells and spatial distribution of the various ion conductances.

Thus, our model has six ion currents, and the membrane potential is described by the following circuit equation:

$$C_m dV/dt = -I_T - I_h - I_{Na} - I_K - I_{Na(P)} - I_L + I_{app}, \quad (1)$$

where $C_m = 1\ \mu F/cm^2$ and I_{app} is the injected current (in $\mu A/cm^2$). The six intrinsic currents are specified as follows.

T-type calcium current

$I_T = g_T \cdot s_\infty^3(V) \cdot h \cdot (V - V_{Ca})$. This is a simplified version of a quantitative kinetic model of I_T,[35] constructed from the voltage-clamp data of Ref. 4. The activation variable s is relatively fast and is replaced by its equilibrium function $s_\infty(V) = 1/(1 + \exp(-(V + 65)/7.8))$. The inactivation variable h obeys an equation of the form:

$$dX/dt = \phi_x(X_\infty(V) - X)/\tau_x(V), \quad (2)$$

where $X = h$, $h_\infty(V) = 1/(1 + \exp((V - \theta_h)/k_h))$, $\tau_h(V) = h_\infty(V)\exp((V + 162.3)/17.8) + 20.0$, and the temperature factor ϕ_h scales the time constant of h (we set $\phi_h = 2$). $g_T = 0.3$–$1.0\ mS/cm^2$ and $V_{Ca} = +120\ mV$.

Sag current

The expression of I_h is taken from Ref. 21: $I_h = g_h \cdot H^2 \cdot (V - V_h)$ (for a different model of I_h, see Ref. 7). The activation variable H obeys Eq. (2), with $H_\infty(V) = 1/(1 + \exp((V + 69)/7.1))$, $\tau_H(V) = 1000/(\exp((V + 66.4)/9.3) + \exp(-(V + 81.6)/13))$ and $\phi_H = 1$. Note that τ_H has a maximum of 1000 ms at $V = -74.5\ mV$, H is quite slow. $g_h = 0.04\ mS/cm^2$ and $V_h = -40\ mV$.

Hodgkin–Huxley currents

Due to the lack of voltage-clamp data for all the currents responsible for spike generation, we will use a simplified form of the Hodgkin–Huxley I_{Na} and I_K.[8,13,23,24] The thresholds of these currents are adjusted by the parameters σ_{Na} and σ_K below. The potassium current $I_K = g_K \cdot n^4 \cdot (V - V_K)$, where n satisfies Eq. (2), with $n_\infty = \alpha_n/(\alpha_n + \beta_n)$, $\tau_n = 1/(\alpha_n + \beta_n)$, $\alpha_n(\sigma_K, V) = -0.01(V + 45.7 - \sigma_K)/(\exp(-0.1(V + 45.7 - \sigma_K)) - 1)$ and $\beta_n(\sigma_K, V) = 0.125\exp(-(V + 55.7 - \sigma_K)/80)$. $\phi_n = 200/7$, $g_K = 30\ mS/cm^2$ and $V_K = -80\ mV$.

The sodium current $I_{Na} = g_{Na} \cdot m_\infty^3(\sigma_{Na}, V) \cdot (0.85 - n) \cdot (V - V_{Na})$, where the inactivation h is replaced by $(0.85 - n)$ following the empirical observation by FitzHugh that during spike generation the kinetic variables h and n satisfy approximately the linear relationship $n + h = 0.85$.[8] Moreover, the activation kinetics being fast, the variable m is replaced by its equilibrium function, $m_\infty = \alpha_m/(\alpha_m + \beta_m)$, $\alpha_m(\sigma_{Na}, V) = -0.1(V + 29.7 - \sigma_{Na})/(\exp(-0.1(V + 29.7 - \sigma_{Na})) - 1)$ and $\beta_m(\sigma_{Na}, V) = 4\exp(-(V + 54.7 - \sigma_{Na})/18)$. $g_{Na} = 42\ mS/cm^2$ and $V_{Na} = +55\ mV$.

Persistent sodium current

$I_{Na(P)}$ is similar to I_{Na}, but without inactivation. We shall assume $I_{Na(P)} = g_{Na(P)} \cdot m_\infty^3(\sigma_{Na(P)}, V) \cdot (V - V_{Na})$ (cf. Ref. 26), with $g_{Na(P)} = 9\ mS/cm^2$. This current activates at a lower level of membrane potential depolarization than I_{Na}, below but close to the spike threshold. The present model is such that, without $I_{Na(P)}$, the I_T-dependent rebound excitation alone cannot reach the spike threshold.

Leak current

$I_L = g_L \cdot (V - V_L)$ represents the sum of all passive currents, including a potassium leakage.[10,19] The reversal potential V_L is largely responsible for setting the resting level of the cell, and the conductance g_L determines the passive time constant of the membrane ($\tau_0 = C_m/g_L$). We shall see that a change of τ_0 may qualitatively alter the behavior of the cell.

In summary, our model neuron is described by only four time-dependent variables: the membrane potential V [Eq. (1)], and three gating variables [Eg. (2), $X = h$, H and n]. This set of four differential equations was integrated numerically using a fifth-order Runge–Kutta method with adaptive stepwise control. Some simulations have been verified by a Gear method with double precision.

RESULTS

Response to rhythmic hyperpolarization

The model was tested first by comparing its response to an injected current pulse with experimental measurements. It fires repetitive Na^+ spikes upon sufficient depolarization, and displays a low threshold spike (LTS) following a hyperpolarization pulse of long duration (not shown). In this set of simulations, the following parameter values were used: $\theta_h = -81\ mV$, $k_h = 6.25\ mV^{-1}$, $g_T = 0.3\ mS/cm^2$ (cf. Ref. 35); $\sigma_{Na} = 3$, $\sigma_{Na(P)} = -5$ and $\sigma_K = 10\ mV$, so that the half-activation points for I_{Na}, $I_{Na(P)}$ and I_K are, respectively, -27, -35 and $-34\ mV$; $g_L = 0.1\ mS/cm^2$, thus $\tau_0 = 10\ ms$ (cf. Ref. 11) and $V_L = -72\ mV$, so that in the absence of I_{app} the cell is at rest with $V = -65.7\ mV$.

With these parameter values, the model neuron does not display slow oscillations under constant injected current, hence it is type I. When a hyperpolarizing current pulse is applied repetitively, the cell responds to the periodic input by LTSs. Since the removal of the I_T inactivation by hyperpolarization is slow, the amplitude of the rebound excitation (LTS) will be small when the cell is driven at high frequencies, possibly too small to reach the threshold of action potentials. To assess the cell's frequency following capability, the parameters of the injected current I_{app} were varied systematically, and the response of the cell was measured as the number (N) of action potentials it generates per period of stimulation. The injected current is specified by three quantities, the intensity I_{app}, the period P_0 and the duration of hyperpolarization p [thus, it is ON for an amount of time p, then OFF for the rest of the period $(P_0 - p)$].

In Fig. 1, the response (N = number of fast Na^+ spikes per period) is plotted as a function of the driving frequency $1/P_0$ and the ratio p/P_0 of the current pulse duration over the period (with $I_{app} = -1.0$). Indeed, one sees that for $1/P_0$ larger than 15 Hz, the response is always subthreshold, $N = 0$. As $1/P_0$ is decreased, the LTS response grows and begins triggering spikes. For a fixed $1/P_0$, say $1/P_0 = 10$ Hz, the maximal response is located at an intermediate value of p/P_0: if this ratio is close to 0, the hyperpolarizing pulse is too brief to deinactivate I_T, while if it is close to 1, the interpulse time window becomes too narrow to allow an LTS response to be fully developed. Thus, had we plotted the number of spikes per period (N) vs p/P_0 (ranging from 0 to 1), we would have obtained a curve similar to what has been measured experimentally *in vitro* from thalamic relay cells of the guinea-pig lateral geniculate nucleus using the same type of protocol (see Fig. 3 in Ref. 18).

For fixed p/P_0 (e.g. equal to 0.6), the response (N) is initially increased with the decrease of the driving frequency $1/P_0$, as is expected from the kinetic properties of the I_T deinactivation. As $1/P_0$ is decreased further beyond 2–3 Hz, however, N starts to decrease again, until $N_0 = 2$ for $1/P_0 < 0.5$ Hz. This reversal of the trend has its origin in the presence of the hyperpolarization-activated sag current I_h. This inward

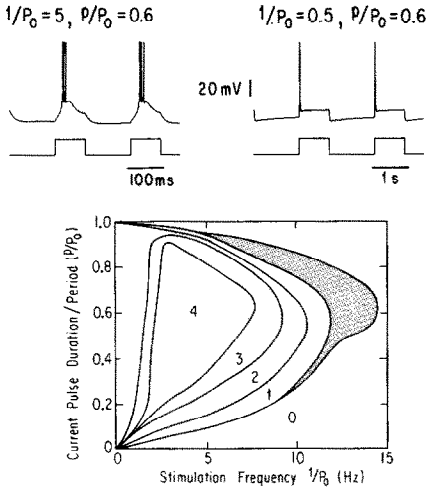

Fig. 1. Response of the model neuron to rhythmic hyperpolarizations at frequency $1/P_0$. In each period the applied current is ON at $-1.0\,\mu A/cm^2$ for p ms, then OFF for $(P_0 - p)$ ms. Upper panel: two examples with $P_0 = 5$ and 0.5 Hz ($p/P_0 = 0.6$). Note the sag depolarization during the hyperpolarizing pulse with $p = 1600$ ms, but not $p = 160$ ms. Lower panel: number of Na^+ spikes elicited per stimulation period ($N = 0, 1, 2, 3, 4$) as a function of $1/P_0$ and p/P_0. $N = 0$ if the driving frequency is higher than 15 Hz. N decreases again for low driving frequency due to the hyperpolarization-activated inward (sag) current. The shaded region corresponds to N smaller than one (e.g. $N = 0.5$ if $1/P_0 = 13$ and $p/P_0 = 0.6$). With the parameter values used here, no bursting oscillation can be produced by constant applied current. $\theta_h = -81$ mV, $k_h = 6.25\,mV^{-1}$, $g_T = 0.3\,mS/cm^2$, $\sigma_{Na} = 3$, $\sigma_{Na(P)} = -5$ and $\sigma_K = 10$ mV, $g_L = 0.1\,mS/cm^2$, $V_L = -72$ mV.

current has a fairly small maximal conductance g_h and its activation is very slow. Therefore, I_h becomes manifest only if the injected current has a sufficiently low frequency and long pulse duration. When this happens (in the small $1/P_0$ range), I_h induces a slow, depolarizing rectification of the membrane potential during a hyperpolarizing pulse. As a result, at the termination of the pulse, the membrane potential is less hyperpolarized than it would be in the absence of the sag current I_h (compare the two time courses in the upper panel of Fig. 1). Since the deeper the hyperpolarization, the larger the peak of the rebound LTS,[11,35] the response amplitude (or N) falls off for very low driving frequencies.

One can determine the value of N in the limit of zero stimulation frequency in the following manner. For any fixed ratio p/P_0, the stimulation duration p becomes increasingly large as $P_0 \to \infty$. With sufficiently long hyperpolarization the neuron converges to a steady state corresponding to constant $I_{app} = -1.0$, in the present case with $V \simeq -73.9$ mV. Therefore, the number of action potentials per period as $1/P_0 \to 0$ is the same as that elicited by the release from a constant hyperpolarizing current, which in the present case is 2. Note that our reasoning does not hold if p/P_0 is not fixed, when P_0 and p/P_0 tend to zero simultaneously. In fact, given an arbitrarily small $1/P_0$, one can choose accordingly small p/P_0 such as p remains about 100 ms or less, so that the effects of I_h are unimportant. This explains why the regions with $N = 3$, 4 extend to the corner near $(1/P_0 = 0, p/P_0 = 0)$ in Fig. 1.

On the $(1/P_0, p/P_0)$ plan, therefore, regions corresponding to fixed values of N ($N = 1$–4) form a curious target-like topology. The entire diagram shows that the model neuron responds optimally (resonantly) to rhythmic hyperpolarization within a frequency range (0.5–14 Hz) which is determined by both the T-type Ca^{2+} current and the non-specific cation sag current. This frequency range is the same as that of the sleep spindle and delta rhythmic burstings observed in the thalamic relay cells.

The "intermittent phase-locking" phenomenon

In the $(1/P_0, p/P_0)$ diagram of Fig. 1, there is a shaded region which corresponds to the case where the number of Na^+ spikes per stimulation period N is not zero but less than one. We found that this presented a generic response, especially if the stimulation frequency was high (around 10 Hz rather than 3 Hz). To illustrate this, let us fix the frequency at $1/P_0 = 10$, and study the response properties of the neuron as a function of the maximal T-conductance g_T and the intensity of the injected current I_{app}. For definiteness we shall let $p/P_0 = 0.8$.

Consider first $g_T = 0.3$. As I_{app} was varied from 0.0 to -2.0, we found a rich variety of response patterns. The response is never superthreshold at every cycle of the periodic stimulation (it can become so if I_{app} is even stronger). On the other hand, a superthreshold

burst may contain more than one Na^+ spike. As a consequence, the different response patterns cannot be distinguished from one another merely by N, the average spiking rate per period. For instance, if the response alternates between being subthreshold with zero spike and superthreshold with two spikes, its average spiking rate is $N = 1$, but it is different from the response which is superthreshold with one spike at each cycle. We shall denote the former pattern by the symbolic name (02) and the latter by (1). Patterns with quite complicated symbolic names were observed. Three examples for $g_T = 0.3$ are shown in Fig. 2A, with the respective symbols (02), (0^340^2203) and (0^230203). With I_{app} incremented by -0.05, all the observed patterns were classified according to their symbolic names (see Table 1). In Table 1 we see that several distinct patterns with $N = 1$ exist. Being

Table 1. Response to rhythmic hyperpolarization ($g_T = 0.3$, $P_0 = 10$ Hz, $p/P_0 = 0.8$)

Current intensity	Response type	Number of Na^+ spikes/period
0.0 to −0.75	0	0
−0.8	0^31	1/4
−0.85	$0^31(01)^4$	5/12
−0.9 to −0.95	01	1/2
−1.0	$02(01)^2$	2/3
−1.05 to −1.1	0201	3/4
−1.15	$(02)^301$	7/8
−1.2 to −1.3	02	1
−1.35	0301	1
−1.4	02	1
−1.45	0301	1
−1.5	0^340^2203	1
−1.55	0^2203	1
−1.6 to −1.65	0^230203	8/7
−1.7 to −1.85	0^24	4/3
−1.9 to −2.0	0^25	5/3

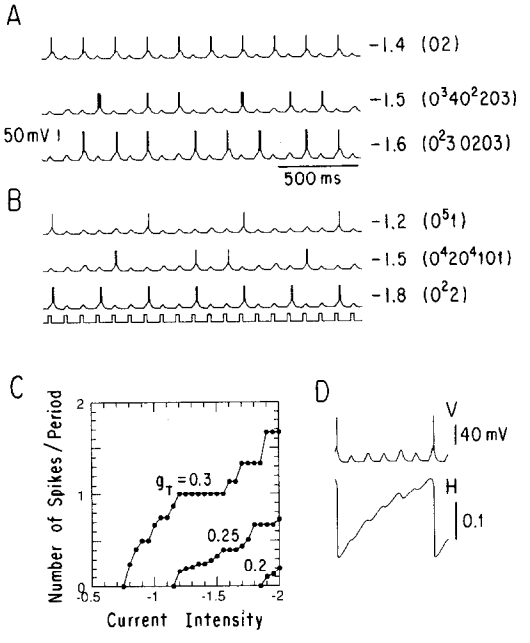

Fig. 2. Response of the model neuron to rhythmic hyperpolarization at $1/P_0 = 10$ Hz and $p/P_0 = 0.8$. Six examples are shown with $g_T = 0.3$ in A and 0.25 in B. Each pattern is classified by a symbolic name which is given on the right hand side of the time course together with the corresponding I_{app} value. For instance, with $g_T = 0.25$ and $I_{app} = -1.8$, the response pattern denoted by (0^22) consists of two subthreshold (0 spike) cycles followed by a burst of two spikes. The responses are not superthreshold at every cycle of the stimulation, but intermittent bursts are all phase-locked to the stimulus. This phenomenon is called "intermittent phase-locking". (C) The number of Na^+ spikes per stimulus period as a function of I_{app} for $g_T = 0.3$, 0.25 and 0.2. This function presents several plateaus and is of staircase-like form with $g_T = 0.3$; it seems smoother with $g_T = 0.25$. Note also that for smaller g_T, larger hyperpolarizing current intensity is required for eliciting superthreshold rebound LTSs. (D) Time course of the membrane potential and the I_h activation variable H with $g_T = 0.25$ and $I_{app} = -1.2$, showing that the quantity H is incremented by each of the five subthreshold cycles leading to a superthreshold event. This indicates that the intermittent phase-locking originates from a temporal integration of hyperpolarizations by the slowly activating sag current.

representable by finite symbolic strings implies that these response patterns are periodic. [For instance, the pattern (0^340^2203) has a period nine times that of the stimulation period]. For period patterns N is always a rational number. When N is plotted vs I_{app}, a non-decreasing function with a number of plateaus is obtained (Fig. 2C). It is conceivable that every point in the diagram is part of a plateau whose width can be resolved only by increasingly small increments of I_{app}, and that between every pair of plateaus there exists yet another plateau of even smaller width, so that the function is reminiscent of a "devil staircase".[9]

When the maximal T-conductance g_T is smaller, stronger hyperpolarization is needed to elicit superthreshold LTSs. This is demonstrated by computing N as a function of I_{app}, with $g_T = 0.25$ and 0.2, and by comparing the two curves with that of $g_T = 0.3$ (Fig. 2C). Figure 2B also shows three examples with $g_T = 0.25$, corresponding to the symbolic names (0^51), (0^420^4101) and (0^22). We have found a few cases with $I_{app} = -1.6$ to -1.75, where the response pattern appeared aperiodic, but this could not be ascertained within the precision of our numerical methods.

Therefore, our simulations revealed that under phasic hyperoparization at 10 Hz, the model neuron can display a remarkable richness of response patterns. All of them share the common feature of not being superthreshold at every cycle of the stimulation. So with repetitive inputs, the neuron usually skips one or more cycles before emitting a burst of Na^+ spikes again. The degree of intermittency of the response patterns depends on the maximal T-conductance g_T, the maximal h-conductance g_h, and the hyperpolarization intensity I_{app}.

This intermittent response can be understood as follows. Suppose that, due to the relatively small conductance and limited deinactivation by a hyperpolarizing step of 80 ms, the rebound excitation produced by I_T alone would be subthreshold. Each hyperpolarizing pulse, however, induces an incremental activation of I_h. As a result of the slowly accumu-

lated I_h after several cycles, the rebound excitation at the next cycle may now reach the threshold of Na^+ spikes. The critical role played by I_h in the intermittent response was confirmed by direct observation of the time course of its activation (Fig. 2D), by the absence of the phenomenon if the stimulation frequency was much lower (e.g. around 3 Hz), if the maximal T-conductance was larger or if I_h was blocked ($g_h = 0$).

Transition from subthreshold to bursting oscillation via chaos

After moderate change of a few parameter values, the model system becomes capable of bursting oscillations under constant injected current. The parameter values used here differ from the previous ones as follows. We have $\theta_h = -79$ mV, $k_h = 5\ \text{mV}^{-1}$ and $g_T = 1\ \text{mS/cm}^2$, so that the low threshold Ca^{2+} current is stronger. Note that more recent voltage-clamp data yield an I_T inactivation equilibrium curve that is steeper than found previously ($k_h = 4.0$ in Ref. 10 compared to 6.3 in Ref. 4). This, together with only a 2 mV positive shift of the $h_\infty(V)$ curve, was found to significantly facilitate the I_T-dependent rhythmogenesis. Besides, the maximal conductance g_T is now about three-fold higher than the previous value, and similar to the values used in Refs 21 and 33. This quantity is likely a variable for thalamic relay cells in different nuclei, from cell to cell in a same nucleus, or even from one part to another part of a single cell once the morphology of the cell is taken into account. Hence it is important to explore how the model's behavior depends on the g_T value. Because of the more powerful I_T, the threshold of I_{Na} is slightly higher ($\sigma_{Na} = 6$ instead of 3 mV). For the leak current, $g_L = 0.12\ \text{mS/cm}^2$ and $V_L = -70$ mV, so that in the absence of I_{app} the cell is at rest with $V = -60.5$ mV.

Before reporting simulation results with $g_T = 1.0$, let us note that intrinsic oscillations cannot be realized if g_T is smaller than a critical value near 0.6. For $g_T < 0.5$, no sustained bursting oscillation at either 10 or 3 Hz is possible, so we go back to the type I case. This holds true regardless of the value of the maximal h-conductance g_h or the constant hyperpolarization intensity I_{app}.

The temporal behaviors of the membrane potential as a function of the injected current intensity, with $g_T = 1.0$, are displayed in Fig. 3. When the cell is depolarized sufficiently from the rest ($I_{app} = 0$) it produces repetitive firing of action potentials ($I_{app} = +3$). The firing rate is about 100 Hz, comparable with the experimental data (see Fig. 2E in Ref. 18). On the other hand, when it is hyperpolarized, the deinactivation of I_T destabilizes the resting state and a subthreshold slow oscillation appears ($I_{app} = -0.45$). This transition occurs through a Hopf bifurcation,[9] where the oscillatory state emerges from a steady state in a continuous and smooth way, so that near the transition the oscillation has an arbitrarily small amplitude, and hence must be subthreshold. Besides, it emerges with a well defined and finite frequency, which in the present case is about 16.5 Hz. With increasing intensity of hyperpolarization, the amplitude of the slow oscillation grows, eventually reaches the spike generation threshold and periodic bursting discharges are elicited. A regular bursting discharge pattern of a period of 83.3 ms (frequency 12 Hz) is displayed in Fig. 3 ($I_{app} = -0.8$). There are four spikes per period (i.e. per LTS); the intraburst spike frequency is 300–400 Hz, except for the interval between the last two spikes of the burst which is more prolonged (about 5 ms; see Fig. 2 in Ref. 18, and Ref. 14). When hyperpolarization is further increased, the bursting oscillation slows down (in Fig. 3, for instance, the frequency is 3.8 Hz at $I_{app} = -1.3$ and 1.7 Hz at $I_{app} = -1.4$). The frequency change as function of I_{app} will be discussed in detail below. The bursting oscillation ceases to exist for $I_{app} \leqslant -2$, and the cell is settled at a steady state of a hyperpolarized level ($V = -76$ mV at $I_{app} = -2.0$).

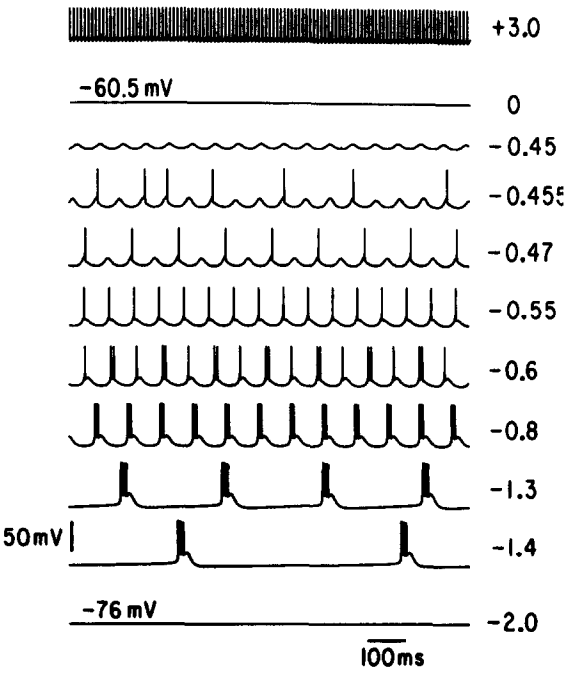

Fig. 3. Dynamic behaviors of a model neuron which is able to display both the spindle-like and delta-like rhythms. Six distinct states are observed as I_{app} is varied: (i) repetitive firing, (ii) resting state, (iii) subthreshold oscillation, (iv) "10 Hz" (7–16 Hz) bursting, (v) "3 Hz" (0.3–4 Hz) bursting and (vi) hyperpolarized steady state. Parameter values differ from those in Figs 1 and 2 as follows: $\theta_h = -79$ mV, $k_h = 5\ \text{mV}^{-1}$, $g_T = 1\ \text{mS/cm}^2$, $\sigma_{Na} = 6$ mV, $g_L = 0.12\ \text{mS/cm}^2$, $V_L = -70$ mV.

Near the onset of bursting oscillations, a few intermediate cases between $I_{app} = -0.45$ and -0.8 are illustrated in Fig. 3. The number N_s of spikes per period of slow oscillation (i.e. per LTS) provides a quantitative measure of the transition between subthreshold oscillation ($N_s = 0$) and bursting oscillation ($N_s > 0$). This number is smaller than one at the onset

of the transition, where there exist a number of oscillatory patterns in which the membrane potential undergoes subthreshold LTSs, only occasionally with one Na^+ spike at the crest of the LTS ($I_{app} = -0.455$ and -0.47 in Fig. 3). Moreover, even when N_s is larger than one, it may be a non-integer (e.g. $N_s = 1.5$ at $I_{app} = -0.6$).

The nature of the transition from the subthreshold to bursting oscillation is not well understood. Two interesting phenomena have been observed in the transition range of I_{app} values. First, there is hysteresis. Indeed, subthreshold and suprathreshold oscillations can co-exist and be stable for the same I_{app} value (Fig. 4A). This can be shown by the following protocol: a constant injected current of the same amplitude is preceded by a current pulse of two different levels, so that the membrane potential is first set to slightly different initial conditions, then subject to an identical current stimulation. A bistability is manifested as two distinct discharge patterns obtained with the same stimulation but different initial conditions (Fig. 4B). From Fig. 4B, we see that the two co-existing states are distinguished by the level of the I_h activation. Indeed, the hysteresis disappears altogether if the sag current is "switched off" ($g_h = 0$). This is a surprising and subtle effect, since in this I_{app} range the membrane potential barely reaches (and only briefly) the I_h activation threshold ($V_{min} \simeq -70$ mV).

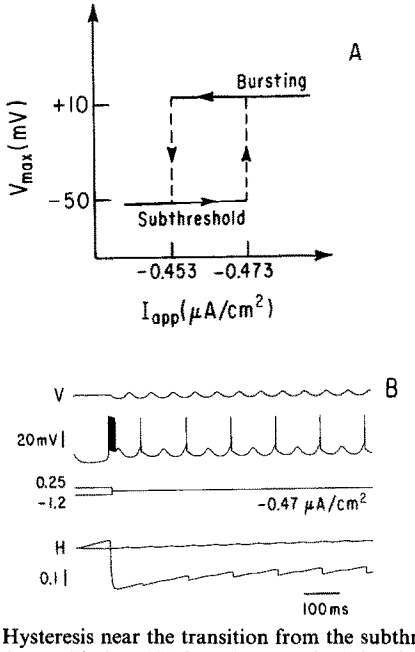

Fig. 4. Hysteresis near the transition from the subthreshold to bursting oscillation. (A) Co-existence of subthreshold and suprathreshold oscillatory states over a narrow range of I_{app}. (B) An example of bistability. A sustained applied current ($I_{app} = -0.47$) is preceded by a current pulse of 100 ms. Two distinct states are observed depending on the amplitude of the initial current pulse ($I_{app} = 0.25$ or -1.2). Note that the two states correspond to different levels of the activation H of the sag current.

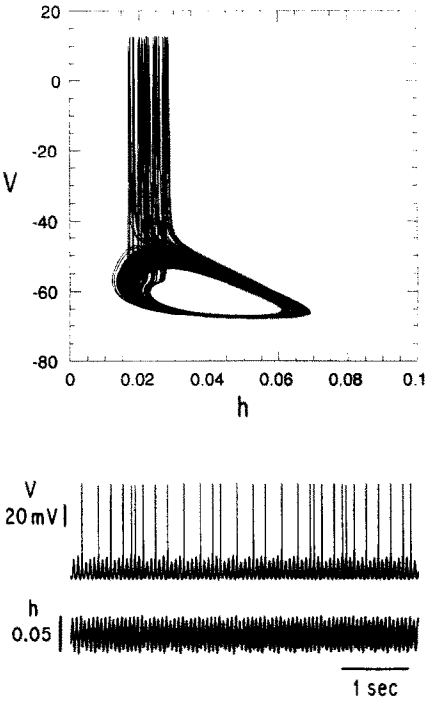

Fig. 5. An apparently chaotic state at $I_{app} = -0.455$. Both the membrane potential V and the inactivation variable h of the T-type calcium current display an aperiodic time course. The mostly subthreshold slow oscillation elicits action potentials only occasionally, at randomly chosen cycles. The plot V vs h reveals a "strange attractor" instead of a simple closed curve in the case of periodic behaviors.

Secondly, irregular (aperiodic) discharge patterns are observed near the onset of rhythmic bursting, as shown in Fig. 3 ($I_{app} = -0.455$). A longer time trajectory of this state is shown in Fig. 5, with both the membrane potential $V(t)$ and the I_T inactivation variable $h(t)$. What is irregular here is the number of subthreshold cycles between each successive pair of Na^+ spike events. Recall that our model is a completely deterministic dynamic system, thus the apparent aperiodicity is an indication of deterministic chaos.[9] Also plotted in Fig. 5 is V vs h. Instead of a simple closed curve of a periodic solution, this "phase portrait" reveals a complicated object (a "strange attractor") typical of a chaotic dynamic state.[9] The same putative chaotic state was observed using the fifth-order Runge–Kutta method, as well as the Gear method with double precision and relative error tolerance of 10^{-14}. So it seems unlikely to be an artifact of numerical integration algorithms with finite precision.

Figure 6 shows another example of chaotic behavior with a few parameter values different from Fig. 5. Here, we used $\theta_h = -75$ mV, which is significantly more positive than the original value of -81 mV. However, we elected to include this figure as an example of intermittent oscillation with characteristics distinct from Fig. 5: following each suprathreshold event (an Na^+ spike), the amplitude

of subthreshold oscillation is virtually nil at the start, then gradually increases until it reaches the spike threshold again. This feature of "spiral chaos" [also evident in the (V,h) plot] is absent in Fig. 5. When we used an alternative expression of I_T due to Huguenard and McCormick,[10] the chaotic state near the transition from the subthreshold to the bursting oscillation was found to be similar to Fig. 6 rather than Fig. 5 (not shown).

Note that the chaotic state of maximal complexity exists only in a small I_{app} range, at the border between the subthreshold oscillation and bursting regimes.

Two bursting modes (3 and 10 Hz)

The model neuron is able to sustain bursting oscillations within a certain frequency range. For the parameter set of Figs 3–5, this frequency range is 0.3–16 Hz, hence the behavior is of type III. The bursting frequency f as a function of the hyperpolarizing current intensity I_{app} is displayed in Fig. 7A (solid circle). Its inverse (the period) is also shown in the same figure (open circle). One sees that the maximal bursting frequency is about 16 Hz. As the hyperpolarization increases, the frequency gradually decreases in almost linear fashion, up to 5 Hz at $I_{app} \simeq -1.25$. Then, a sudden drop of frequency takes place, with $f = 3.8$ Hz at $I_{app} = -1.3$ and 1.7 Hz at -1.4. For I_{app} between -1.4 and -1.9, the frequency f is further decreased up to 0.3 Hz, when the bursting state is taken over by a hyperpolarized steady state (cf. Fig. 3).

The bursting period as function of I_{app} also indicates a quite abrupt change at $I_{app} \simeq -1.25$: it remains relatively constant, then takes off and drastically increases after that point. We shall speak

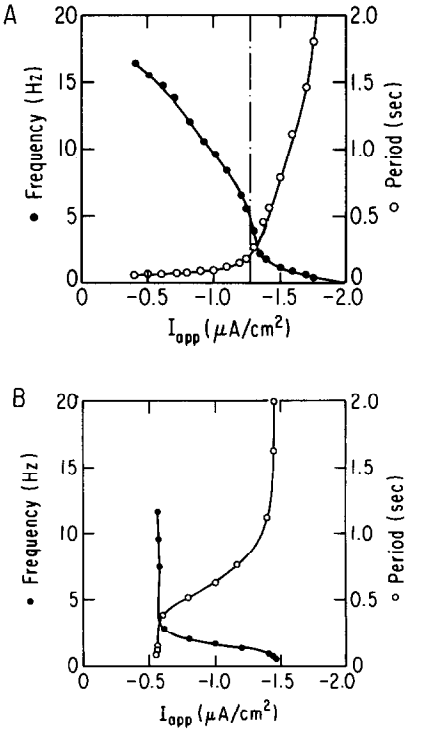

Fig. 7. The frequency (solid circle) and period (open circle) of bursting oscillations vs I_{app}. (A) With the parameter set of Figs 3–5, there is a 5–16 Hz regime and a 0.3–4 Hz regime, separated by a fairly sharp frequency drop. If the sag current is blocked ($g_h = 0$), the 5–16 Hz regime (to the left of the vertical dashed line) remains essentially intact, while the 0.3–4 Hz regime (to the right of the vertical dashed line) is completely destroyed. In B, the faster bursting regime is suppressed when g_T is decreased from 1.0 to 0.7 and g_L from 0.1 to 0.04 mS/cm^2, compared to A. This suggests that the intrinsic conductances may enable a thalamic cell to display only the slower rhythm if g_T is not very strong, and if the passive time constant ($\tau_0 = C_m/g_L$) is sufficiently large.

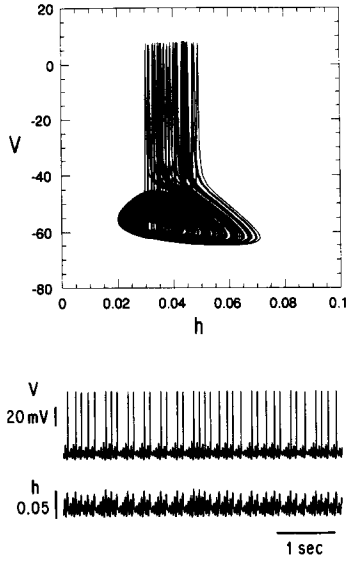

Fig. 6. An example of "spiral chaos". Parameter values differ from those of Figs 3–5 as follows: $\theta_h = -75$ mV, $g_{Na(P)} = 8$, $g_K = 35$, $g_L = 0.08$ mS/cm^2, $I_{app} = -0.95$ μA/cm^2.

of the 10 Hz rhythm for the regime before, and of the 3 Hz rhythm after, the point $I_{app} \simeq -1.25$. The slower, 3 Hz regime is I_h-dependent, while the 10 Hz regime is predominantly not. Indeed, when the sag current is blocked ($g_h = 0$), the 10 Hz regime is basically unaffected (for instance, $f = 6.5$ Hz at $I_{app} = -1.2$, both with or without I_h). However, the 3 Hz regime is completely destroyed in that case (if $g_h = 0$, the cell tends to a steady state for $I_{app} \leqslant -1.3$). Therefore, the transition from 10 to 3 Hz regimes may be explained as follows. In the 10 Hz regime, the oscillation is sustained mainly by the low threshold Ca^{2+} current I_T. Because the membrane potential does not reach a sufficiently negative level, the sag current I_h is not essential. When the applied current reaches a critical strength, I_T alone is no longer strong enough to overcome the hyperpolarization. Thus, in the absence of I_h, the cell would have been inhibited to a hyperpolarized steady state. The sag current, however, becomes significant at this membrane potential range, and may now contribute to depolarize the cell sufficiently so that the escape from hyperpolarization is again possible. Because of the slow I_h

activation, however, the resulting oscillation will have a much longer period than the I_h-independent oscillations. This explains the transition from the 10 Hz rhythm to the 3 Hz one. However, it is not entirely clear what determines the degree of smoothness of the frequency change.

In the *in vitro* slice recordings from thalamic relay cells, only a relatively slow oscillation (0.5–4 Hz) has been observed (type II behavior).[14,20,25] In our model we found that one can readily decrease the maximal bursting frequency, and thereby pass from type III behavior to type II behavior, by moderately decreasing the maximal T-conductance g_T and slowing down the passive membrane process (with a larger τ_0). Without changing τ_0, the inactivation time constant $\tau_h(V)$ of I_T is the most important factor in determining the maximal bursting frequency, while the maximal conductance g_T controls the width of the bursting range of I_{app} values.

Let $g_T = 0.7$ instead of 1.0 mS/cm^2 and $g_L = 0.04$ instead of 0.12 mS/cm^2 (so that $\tau_0 = 25$ ms). [In Ref. 19, $\tau_0 \simeq 15$ ms (respectively 45 ms) for thalamic relay cells in rat (respectively in cat).] Then, when we reconstruct the function of the bursting frequency f vs I_{app} (Fig. 7B), we see that the 3 Hz regime becomes dominant over the I_{app} range where the bursting oscillation exists. There still remains a residual 10 Hz regime, in a very narrow range of I_{app} values. This may also be a feature of other models of thalamic relay neuron,[19,33] though it may not be easily detected if I_{app} is not varied with sufficiently small increment. Therefore, we conclude that the distinction between our type II (with only 3 Hz rhythmic bursting) and type III (with both 10 and 3 Hz bursting modes) behaviors is not absolute.

DISCUSSION

Comparison with other models of thalamic relay neurons

Several computational works on thalamic cells have been performed in recent years. Before the voltage-clamp experiments on I_T and I_h, Rose and Hindmarsh modeled single thalamic cells and, among other phenomena, considered the possibility of 10 Hz oscillations in an isolated cell.[24] When the voltage-clamp data became available, a kinetic model of the T-type calcium current was derived, and it was shown that an intrinsic 10 Hz rhythmicity could be generated only by I_T and a leakage current I_L.[35] In a more recent work, the I_T model of Ref. 35 is incorporated into the Rose–Hindmarsh model, which is further analysed mathematically (Rush M. and Rinzel J., unpublished). The slow sag current is not included in these studies. On the other hand, the 3 Hz delta-like oscillation has been modeled in Refs 16, 19, 21 and 33. Here, we report a minimal model of the thalamic relay neuron where both the 10 and 3 Hz bursting modes can be observed.

In this paper we have focused on the essential role played by I_T and I_h in thalamic rhythmogenesis, and did not take into account the effects of several ion channels possessed by the thalamic relay neurons. These include a fast transient potassium current (I_A) with voltage dependence similar to I_T, and a slowly inactivating potassium current identified as the tetraethylammonium-sensitive I_{K2} in the rat ventroposterior relay cells and the 4-aminopyridine-sensitive I_{AS} in the guinea-pig dorsal lateral geniculate relay cells. There also exist calcium-dependent potassium currents, which seem to require the activation of the high-threshold Ca^{2+} current, likely located on the dendrites.[11,12] In Ref. 19 I_A and I_{K2}, as well as a voltage- and calcium-sensitive I_C, are included in a model of thalamic relay neurons. Based on extensive simulations it was concluded that all three K^+ currents contribute to the amplitude–time course of the low threshold Ca^{2+} spikes: I_A to the rising phase, I_C to the initial and I_{K2} to the later repolarizing phase of the LTS. We have performed a limited amount of simulations of our model with the addition of either I_A or I_{K2} from Ref. 10, and found that they contribute significantly to the quantitative sculpturing of the membrane potential's time course, but did not alter the conclusions presented in the Results section.

In our model, the afterhyperpolarization following LTS is produced by I_h inactivation during the depolarizing LTS.[20]

Ionic basis of thalamic oscillations in the spindle/delta frequency range

As the present work illustrates, different balances of the same set of ion channels may lead to distinct repertoires of dynamical states. Therefore, the sole knowledge about the set of ion channels that a thalamic relay cell possesses is not sufficient to predict its behaviors. We have shown for this model system that the T-type Ca^{2+} conductance is critical in both spindle and delta rhythmogenesis: if the maximal conductance g_T is below a threshold value, stable bursting oscillations cannot be generated by a constant applied current. It follows that, due to the variability of g_T, a subgroup of thalamic relay cells in a given population (e.g. of the same nucleus) may be more prone to intrinsic oscillations than others, and may thus subserve initiators of thalamic population rhythms.

The 10 Hz spindle bursting becomes realizable if g_T is sufficiently large and the passive time constant is sufficiently small ($\tau_0 \simeq 10$ ms). In contrast to the 10 Hz bursting mode, the slower 3 Hz mode is critically dependent on the hyperpolarization-activated sag conductance. This is consistent with the experimental observations that the slow 3 Hz rhythm could be abolished by the blockage of either I_T or I_h, and was not observed in relay neurons naturally devoid of I_T.[14] If both the 10 and 3 Hz bursting modes are possible, at different levels of hyperpolarization, we showed that the transition between the two rhythmic

regimes is continuous, although the bursting frequency may present a marked drop near the transition. Therefore, we suggest that the two rhythmic modes form part of a continuous spectrum of cellular behaviors in the relay neurons. Due to their different dependence on I_T and I_h, however, they may be modulated by transmitters and pharmacological agents in a different way.

The 10 Hz mode was suppressed, and the 3 Hz mode became dominant, when the maximal T-conductance g_T was smaller and the passive time constant τ_0 larger (Fig. 7). It would be interesting to compute experimentally the bursting frequency vs current intensity curve, and see if both kinds shown in Fig. 7 could be realized by different subgroups of relay neurons. With fixed g_T and τ_0 values, the maximal bursting frequency is largely limited by the inactivation time constant $\tau_h(V)$ of I_T. Indeed, we have done simulations with Huguenard–McCormick's expression of I_T,[10] which has a somewhat larger $\tau_h(V)$. Most of the results reported here were reproduced, but the maximal bursting frequency was found to be about 10 Hz (instead of the 16 Hz in Fig. 7) and the frequency change to the 3 Hz regime is smoother.

Both rhythmic modes discussed here are elicited by hyperpolarization, and the required hyperpolarization is within the range of membrane potential values observed in thalamic relay neurons during electroencephalogram-synchronized sleep.[30] The present computational results agree with the notion that the delta rhythm appears in relay cells at more hyperpolarized membrane potentials than the spindle rhythm.[22,28] The gradually increased hyperpolarization of thalamic relay cells, during the transition from arousal to the spindle-related early stages then to the delta-related later stages of quiet sleep, is ascribed to the removal of depolarizing pressures from the brainstem as well as the neocortex.[17,30]

Intermittent phase-locking and temporal integration of hyperpolarizations

During *in vivo* spindling 10 Hz oscillations, the thalamic relay neurons remain subthreshold for most of the rhythmic cycles, and only occasionally reach the Na^+ spike threshold to emit a burst of action potentials. This was already noticeable in early intracellular recordings by Andersen and Sears (Fig. 3 in Ref. 2), was repeatedly observed by Steriade and his colleagues (see Figs 2C and 4 in Ref. 6, Fig. 2 in Ref. 27 and Fig. 1 in Ref. 29), and was also shown in the first *in vitro* observation of spindle-like oscillations in thalamic slices (Fig. 1 in Ref. 34). In extracellular measurements, a single unit emits bursts of Na^+ spikes only sparsely in time. Hence, the oscillation may appear non-rhythmic, but the bursting is always phase-locked with the population rhythmicity measured by the local field potentials (Fig. 4 in Ref. 3). Such "intermittent phase-locking" represents one of the most conspicuous characteristics of thalamic relay neurons during the spindle oscillations, yet the cellular or network mechanism(s) have not been elucidated. An interesting experiment showed that when a relay cell was subject to repetitive injection of hyperpolarizing pulses, the response reached the Na^+ spike threshold only intermittently (Fig. 10 of Ref. 31), suggesting that the intermittent behavior is an intrinsic cellular property and involves a time integration of hyperpolarizations.

In this study, we identified two mechanisms for the spindle's intermittent oscillations. The first occurs when the model neuron is capable of an intrinsic 10 Hz oscillation. Near the transition from subthreshold to bursting rhythmic regimes, an apparently chaotic oscillation was observed, where single Na^+ spikes are triggered only at randomly chosen cycles of a mostly subthreshold slow oscillation (Figs 5, 6). Although this happens only for a narrow parameter range, we found that its existence near the onset to bursting oscillations was robust against structural variations of the model. For instance, it persisted when the activation variable of I_T was assumed to obey its actual kinetics rather than being an instantaneous function of the membrane potential. It was also observed using Huguenard–McCormick's expression of I_T (not shown). The phenomenon is inherently non-linear and difficult to interpret intuitively. A more detailed analysis seems worthwhile for the understanding of this transition and the resulting bursting oscillations themselves, especially because the bursting oscillations discussed here differ from another class of neuronal bursting, where the slow oscillation originates from a process (e.g. activation of a calcium-dependent potassium current) which is gradually built up by fast action potentials. Here, the slow oscillation is independent of the Na^+ spikes.

The second form of intermittent oscillation occurs as a response to rhythmic hyperpolarization, when the model neuron is not intrinsically oscillatory (Fig. 2). After a burst of Na^+ spikes, the neuron typically remains subthreshold for one or several stimulation cycles, before becoming superthreshold again. A remarkable variety of such intermittent response patterns have been revealed (Fig. 2, Table 1). As we showed in the Results section, this phenomenon is dependent on the hyperpolarization-activated I_h. More specifically, the slow I_h activation integrates hyperpolarization pulses that are presented rhythmically at about 10 Hz, thereby producing an accumulated depolarization over several periods of the stimulus. Without this sag depolarization the T-conductance alone would not be able to produce a rebound LTS strong enough for the cell to reach the Na^+ spike threshold, and even with the help of I_h, it can do so only once in a while.

This I_h-dependent effect is quite robust, as shown in Fig. 2. It was also observed when Huguenard–McCormick's expression of I_T was used, and when the cell being driven was capable of the slower 3 Hz intrinsic oscillation (Wang X.-J. and Rinzel J.,

unpublished). On the other hand, the effect was found to be absent when the intrinsic 10 Hz bursting oscillation was possible, perhaps because a larger g_T value rendered the accumulated depolarization unnecessary for the cell to reach the Na^+ spike threshold. Since the intermittent response patterns found in the present work present strong similarities with intracellular recordings from thalamic relay cells during spindle oscillations, we hypothesize that the h-conductance provides a key cellular substrate for the intermittent phase-locking phenomenon observed experimentally in those cells, with the rhythmic hyperpolarization being inhibitory postsynaptic potentials of the reticular nucleus origin.

Concomitantly with the intermittent effect, our simulations revealed other unusual dynamic properties of the model neuron which are also I_h sensitive. In particular, the interesting target-like pattern summarizing the frequency following capability of the cell (Fig. 1, lower panel) is subject to direct laboratory verification (we are not aware of intracellular recordings of the thalamic relay cell subject to stimulations at very low frequency).

It was recently suggested that the slow hyperpolarization-activated I_h may provide a mechanism for "subharmonic phase-locking" in central pattern generators,[15a] and may be relevant to certain types of brain rhythms as well (Kopell N., personal communications). The present work showed that the h-conductance is indeed capable of giving rise to such a phenomenon. With the I_h kinetics presently used, this intermittent effect is probably unimportant if the rhythmic drive is either much lower or higher than 10 Hz (cf. Fig. 1). At lower frequency (say 3 Hz), the hyperpolarization duration is comparable to the time scale of the I_h activation, so the latter should saturate in one cycle and cannot accumulate over several cycles. At higher frequency (say 20–40 Hz), on the other hand, each hyperpolarizing pulse would be too brief to activate any significant amount of I_h, and the limited activation would be cancelled out during the release or depolarizing phase of the cycle. Therefore, given an I_h with specified gating kinetics, it can produce the intermittent phase-locking phenomenon within a particular range of the rhythmic driving frequency. In the case of thalamic relay neurons, this range is that of the 10 Hz spindle oscillations. In addition to the h-conductance, the participation of the T-conductance is also critical, and the two of them operating together give rise to a plethora of complex and intermittent response discharge patterns. Note that, in general, this phenomenon does not require that the observed cell be driven by an autonomous pacemaker. In the thalamic network, the repetitive hyperpolarization would originate from the reticular nucleus. The intermittent phenomenon is still expected in thalamic relay cells, if the rhythmic synaptic transmission is a result of the network interactions between these cells and the GABAergic reticular cells.

CONCLUSIONS

The present study showed that the interplay between I_T and I_h provides a cellular substrate for thalamic rhythmic activities, and identified the conditions on the membrane parameter values that are necessary for the intrinsic oscillations in the spindle frequency (7–14 Hz) and delta frequency (0.5–4 Hz) ranges. Furthermore, it revealed that the same set of ion channels may explain the so-called "intermittent phase-locking" phenomenon characteristic of the thalamic delay cells during spindle oscillations.

The *in vivo* spindle and delta brain waves are network phenomena where other neuronal populations in interaction with the thalamic relay neurons must be taken into account.[1–3,30,34] As already mentioned above, inputs from the thalamic reticular nucleus are probably necessary in generating synchronized population rhythms in the relay nuclei.[3,30,34,36] The cortex is known to be critically involved in the mechanisms underlying the delta slow wave phenomenon.[32] It is hoped that our model of single relay neurons will be expanded and used in a computational study of network rhythmic activities of the spindle and delta types.

Acknowledgements—It is a pleasure to thank L. P. Kadanoff for his support, and J. Rinzel, N. Kopell and M. Rush for discussions. This work is partly supported by the Office of Naval Research under contract No. N00014-90J-1194.

REFERENCES

1. Andersen P. and Andersson S. A. (1968) *Physiological Basis of the Alpha Rhythm.* Appleton-Century-Crofts, New York.
2. Andersen P. and Sears T. A. (1964) The role of inhibition in the phasing of spontaneous thalamo-cortical discharge. *J. Physiol., Lond.* **173,** 459–480.
3. Buzsáki G. (1991) The thalamic clock: emergent network properties. *Neuroscience* **41,** 351–364.
4. Coulter D. A., Huguenard J. R. and Prince D. A. (1989) Calcium currents in rat thalamocortical relay neurons: kinetic properties of the transient, low threshold current. *J. Physiol.* **414,** 587–604.
5. Curró Dossi R., Nuñez A. and Steriade M. (1992) Electrophysiology of a slow (0.5–4 Hz) intrinsic oscillation of cat thalamocortical neurons *in vivo*. *J. Physiol.* **447,** 215–234.
6. Deschênes M., Paradis M., Roy J. P. and Steriade M. (1984) Electrophysiology of neurons of lateral thalamic nuclei in rat: resting properties and burst discharges. *J. Neurophysiol.* **51,** 1196–1219.
7. Destexhe A. and Babloyantz A. (1993) A model of the inward current I_h and its possible role in thalamocortical oscillations. *NeuroReport* **4,** 223–226.
8. FitzHugh R. (1961) Impulses and physiological states in theoretical models of nerve membrane. *Biophys. J.* **1,** 445–466.

9. Glass L. and Mackey M. C. (1988) *From Clock to Chaos: the Rhythms of Life*. Princeton University Press, Princeton, NJ.
10. Huguenard J. R. and McCormick D. A. (1992) Simulation of the currents involved in rhythmic oscillations in thalamic relay neurons. *J. Neurophysiol.* **68,** 1373–1383.
11. Jahnsen H. and Llinás R. R. (1984) Electrophysiological properties of guinea-pig thalamic neurones: an *in vitro* study. *J. Physiol., Lond.* **349,** 205–226.
12. Jahnsen H. and Llinás R. R. (1984) Ionic basis for the electroresponsiveness and oscillatory properties of guinea-pig thalamic neurones *in vitro*. *J. Physiol., Lond.* **349,** 227–247.
13. Krinskii V. I. and Kokoz Yu. M. (1973) Analysis of equations of excitable membranes—I. reduction of the Hodgkin–Huxley equations to a second order system. *Biofizika* **18,** 533–539.
14. Leresche N., Lightowler S., Soltesz I., Jassik-Gerschenfeld D. and Crunelli V. (1991) Low-frequency oscillatory activities intrinsic to cat and rat thalamocortical cells. *J. Physiol.* **441,** 155–174.
15. Llinás R. R. (1988) The intrinsic electrophysiological properties of mammalian neurons: insights into central nervous system function. *Science* **242,** 1654–1664.
15a. LoFaro T., Kopell N., Marder E. and Hooper S. L. (1993) Subharmonic coordination in networks of neurons with slow conductances. *Neural Computation* (in press).
16. Lytton W. W. and Sejnowski T. J. (1992) Computer model of ethosuximide's effect on a thalamic neuron. *Ann. Neurol.* **32,** 131–139.
17. McCormick D. A. (1992) Neurotransmitter actions in the thalamus and cerebral cortex and their role in neuromodulation of thalamocortical activity. *Prog. Neurobiol.* **39,** 337–388.
18. McCormick D. A. and Feeser H. R. (1990) Functional implications of burst firing and single spike activity in lateral geniculate relay neurons. *Neuroscience* **39,** 103–113.
19. McCormick D. A. and Huguenard J. R. (1992) A model of the electrophysiological properties of thalamocortical relay neurons. *J. Neurophysiol.* **68,** 1384–1400.
20. McCormick D. A. and Pape H.-C. (1990) Properties of a hyperpolarization activated cation current and its role in rhythmic oscillation in thalamic relay neurons. *J. Physiol.* **431,** 291–318.
21. McCormick D. A., Huguenard J. R. and Strowbridge B. W. (1992) Determination of state-dependent processing in thalamus by single neuron properties and neuromodulators. In *Single Neuron Computation* (eds McKenna T. *et al.*), pp. 259–290. Academic Press, Boston, MA.
22. Nuñez A., Curró Dossi R., Contreras D. and Steriade M. (1992) Intracellular evidence for incompatibility between spindle and delta oscillations in thalamocortical neurons of cat. *Neuroscience* **48,** 75–85.
23. Rinzel J. (1985) Excitation dynamics: insights from simplified membrane models. *Fedn Proc.* **15,** 2944–2946.
24. Rose R. M. and Hindmarsh J. L. (1989) The assembly of ionic currents in a thalamic neuron (Parts I–III). *Proc. R. Soc. Lond. B* **237,** 267–334.
25. Soltesz iI., Lightowler S., Leresche N., Jassik-Gerschenfeld D., Pollard C. E. and Crunelli V. (1991) Two inward currents and the transformation of low-frequency oscillations of rat and cat thalamocortical cells. *J. Physiol.* **441,** 175–197.
26. Steinberg I. Z. (1988) Computer simulations of the effect of non-inactivating sodium channels on the electric behavior of excitable cells. *J. theor. Biol.* **133,** 193–214.
27. Steriade M. and Deschênes M. (1988) Intrathalamic and brainstem–thalamic networks involved in resting and alert states. In *Cellular Thalamic Mechanisms* (eds Bentivoglio M. and Spreafico R.), pp. 37–62. Elsevier, Amsterdam.
28. Steriade M., Curró Dossi R. and Nuñez A. (1991) Network modulation of a slow intrinsic oscillation of cat thalamocortical neurons implicated in sleep delta waves: cortically induced synchronization and brainstem cholinergic suppression. *J. Neurosci.* **11,** 3200–3217.
29. Steriade M., Curró Dossi R. and Paré D. (1992) Mesopontine cholinergic systems suppress slow rhythms and induce fast oscillations in thalamocortical circuits. In *Induced Rhythms in the Brain* (eds Başar E. and Bullock T. H.), pp. 251–267. Birkhäuser, Boston, MA.
30. Steriade M., Jones E. G. and Llinás R. R. (1990) *Thalamic Oscillations and Signaling*. John Wiley, New York.
31. Steriade M., Deschênes M., Domich L. and Mulle C. (1985) Abolition of spindle oscillations in thalamic neurons disconnected from nucleus reticularis thalami. *J. Neurophysiol.* **54,** 1473–1497.
32. Steriade M., Gloor P., Llinás R. R., Lopes de Silva F. H. and Mesulam M. M. (1990) Basic mechanisms of cerebral rhythmic activities. *Electroenceph. clin. Neurophysiol.* **76,** 481–508.
33. Tóth T. and Crunelli V. (1992) Computer simulation of the pacemaker oscillations of thalamocortical cells. *NeuroReport* **3,** 65–68.
34. von Krosigk M., Bal T. and McCormick D. A. (1993) Cellular mechanisms of a synchronized oscillation in the thalamus. *Science* **261,** 361–364.
35. Wang X.-J., Rinzel J. and Rogawski M. A. (1991) A model of the T-type calcium current and the low-threshold spikes in thalamic neurons. *J. Neurophysiol.* **66,** 839–850.
36. Wang X.-J. and Rinzel J. (1993) Spindle rhythmicity in the reticularis thalami nucleus: synchronization among mutually inhibitory neurons. *Neuroscience* **53,** 899–904.
37. Wilcox K. S., Gutnick M. J. and Christoph G. R. (1988) Electrophysiological properties of neurons in the lateral habenula nucleus: an *in vitro* study. *J. Neurophysiol.* **59,** 212–225.

(*Accepted* 10 *August* 1993)